

SoftShadow: Leveraging Penumbra-Aware Soft Masks for Shadow Removal

Xinrui Wang^{1*}, Lanqing Guo^{2*}, Xiyu Wang¹, Siyu Huang³, Bihan Wen¹

¹Nanyang Technological University, Singapore

²The University of Texas at Austin, USA

³Clemson University, USA

Abstract

Recent advancements in deep learning have yielded promising results for the image shadow removal task. However, most existing methods rely on binary pre-generated shadow masks. The binary nature of such masks could potentially lead to artifacts near the boundary between shadow and non-shadow areas. In view of this, inspired by the physical model of shadow formation, we introduce novel soft shadow masks specifically designed for shadow removal. To achieve such soft masks, we propose a *SoftShadow* framework by leveraging the prior knowledge of pretrained SAM and integrating physical constraints. Specifically, we jointly tune the SAM and the subsequent shadow removal network using penumbra formation constraint loss and shadow removal loss. This framework enables accurate predictions of penumbra (partially shaded regions) and umbra (fully shaded regions) areas while simultaneously facilitating end-to-end shadow removal. Through extensive experiments on popular datasets, we found that our SoftShadow framework, which generates soft masks, can better restore boundary artifacts, achieve state-of-the-art performance, and demonstrate superior generalizability.¹

1 Introduction

Shadow removal aims to restore content obscured in shadow regions and correct degraded illumination. Recently, deep learning methods have shown excellent performance in shadow removal tasks relying on large-scale training data. However, predicting shadow-free results remains challenging due to the highly variable illumination and color distortions in shadow areas. Boundary artifacts are particularly easy to occur because of the complex transitions in illumination at boundary regions, and it is also difficult to precisely locate the shadow areas around the boundary.

A few methods rely on binary shadow masks as input to indicate the shadow regions. These binary shadow masks are either manually annotated (Wang, Li, and Yang 2018; Liu et al. 2024), or predicted by off-the-shelf shadow detectors (Cun, Pun, and Shi 2020). However, obtaining such shadow masks can be costly and complicated, making these methods less desirable for real-world applications. Moreover, binary masks fall short of representing the blurry edges of soft shadows, causing boundary artifacts in removal results. Soft shadows occur when the light source is par-

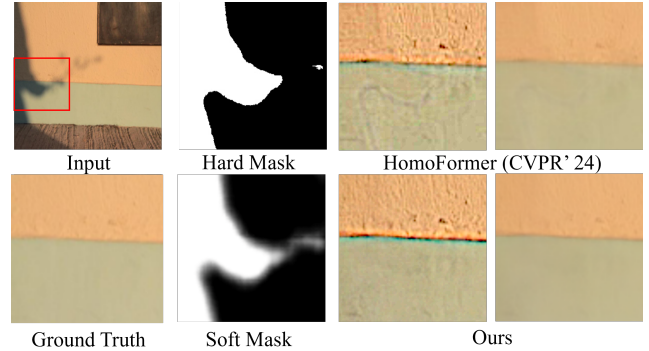


Figure 1: Illustration of soft shadow removal results using our proposed *SoftShadow* with *soft* shadow mask compared to the most recent competing methods HomoFormer (Xiao et al. 2024) using *hard* shadow masks. The third column shows sharpened versions of our results and HomoFormer’s results for better visualization.

tially occluded, resulting in a gradual transition between shadow and non-shadow regions, which is also known as the penumbra area. As shown in Figure 1, when the input image contains soft shadows, the previous state-of-the-art (SOTA) method (Xiao et al. 2024) suffers from boundary artifacts. Other approaches attempt shadow removal without explicitly extracting the shadow mask. Instead, they incorporate semantic parsing modules into shadow removal networks. For instance, some approaches involve predicting degradation attention (Qu et al. 2017; Cun, Pun, and Shi 2020), while others utilize domain classifiers (Jin, Sharma, and Tan 2021; Jin et al. 2024) to better understand and address shadow effects. However, their performance may be limited by the lack of powerful external detectors providing additional shadow location information, and the number of model parameters could increase significantly.

In view of this, we argue that simply leveraging the binary mask to represent the shadow location is not enough. Differently, we introduce a novel soft shadow mask specifically designed for shadow removal as shown in the hard mask *v.s.* soft mask of Figure 1, inspired by the physical shadow for-

*Equal contribution for both authors

¹<https://github.com/Xinrui014/SoftShadow/>

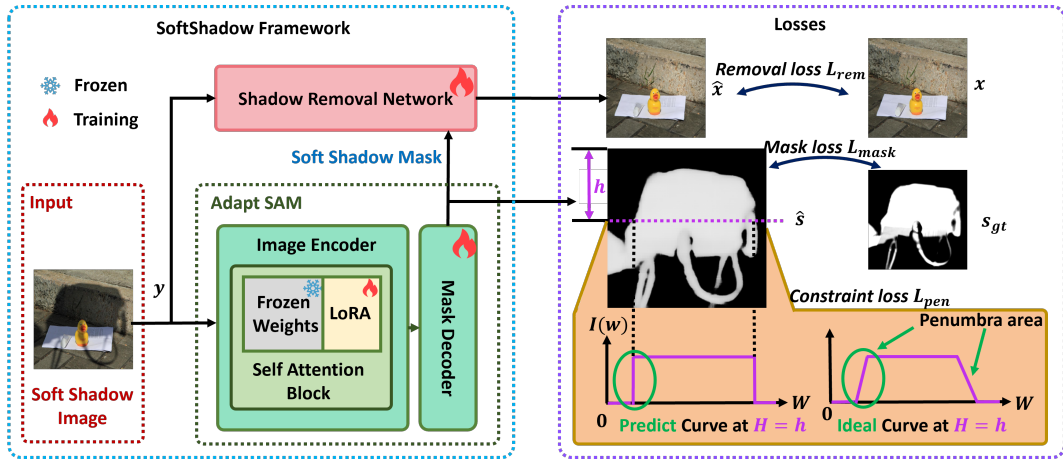


Figure 2: Illustration of the proposed SoftShadow. The **left box** illustrates the SoftShadow architecture, where a shadow image y is input into SAM for detecting soft shadow masks. The shadow removal network then processes the soft mask and the shadow image to produce a shadow-free image. The **right box** shows the three losses we used in SoftShadow. From top to bottom, the removal loss \mathcal{L}_{rem} is calculated between shadow-free images and shadow-removal images. The mask loss \mathcal{L}_{mask} is calculated between predicted soft masks and ground truth soft masks. The constraint loss \mathcal{L}_{pen} is trying to regularize the gradient orientation and magnitude of predicted soft masks in the penumbra area.

mation model. The soft masks can precisely locate the inner and outer boundaries of shadow and indicate the penumbra area with proper degradation variance. Moreover, recognizing the effectiveness of employing a powerful pre-trained detector for providing semantic information, we utilize the prior knowledge from the pre-trained SAM (Kirillov et al. 2023). While existing methods (Zhang, Gu, and Zhu 2023) have used the off-the-shelf SAM in a naive way, merely predicting the shadow mask as input to the shadow removal network, we adapt SAM as a soft shadow mask predictor and jointly optimize it with the shadow removal network.

In this paper, we first propose a unified shadow removal framework, dubbed *SoftShadow*, which removes shadow from images in an end-to-end manner without requiring input shadow masks as shown in Figure 2. We integrate the pre-trained SAM combined with Low-Rank Adaptation (LoRA) (Hu et al. 2021) to jointly adapt the SAM model and shadow removal model at a much lower computational cost compared with the previous methods (Chen et al. 2023). Based on this, the framework enables accurate predictions of soft shadow masks with penumbra as intermediate results while simultaneously facilitating end-to-end shadow removal. Besides, we introduce a penumbra formation constraint to assist SAM adaptation. This constraint regularizes the gradient of the predicted mask in the penumbra area, resulting in more accurate predictions of detailed and spatially varied shadow masks. In the commonly used shadow removal datasets, SRD and LRSS datasets contain soft shadow images, which makes them more suitable for illustrating the improvements of utilizing soft shadow masks. Experimental results show that *SoftShadow* achieves superior performance on SRD and LRSS datasets. Our main contributions are summarized as follows:

- We propose a unified shadow removal framework that

does not require additional input shadow masks, enabling accurate predictions of soft masks as intermediate results, which is specifically designed to capture detailed and spatially varied shadow location information.

- We introduce penumbra formation constraint inspired by physical shadow formation model to further refine the soft mask in the penumbra area. By leveraging the constraint loss and shadow removal loss, we jointly tune the SAM and the subsequent shadow removal network.
- Experimental results demonstrate that SoftShadow surpasses state-of-the-art shadow removal methods on the SRD and LRSS datasets, achieving superior performance and even comparable results with previous methods that use ground truth mask inputs.

2 Related Work

2.1 Shadow Removal

The degradation of shadows varies in each image, posing a significant challenge for shadow image restoration. In recent years deep learning-based approaches have achieved remarkable results in shadow removal (Guo et al. 2024). Some methods restore the shadow image with the guidance of shadow masks. For example, SP+M-Net (Le and Samaras 2019) employs two deep networks to predict shadow matte and shadow parameters. Recently, powerful backbones such as transformers (Vaswani et al. 2017; Dosovitskiy et al. 2020), and diffusion models (Ho, Jain, and Abbeel 2020; Saharia et al. 2022) have been applied to the shadow removal task. HomoFormer (Xiao et al. 2024) homogenizes the spatial distribution of shadow masks to uniformly recover the entire shadow image, while ShadowDiffusion (Guo et al. 2023b) provides a robust generative prior for producing natural shadow-free images. Some methods aim to eliminate the dependency on shadow mask

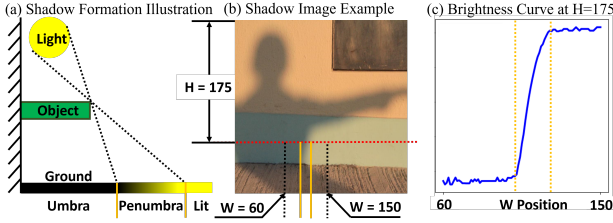


Figure 3: (a) Illustration of the shadow formation geometry that creates the penumbra and umbra (Nielsen and Madsen 2007).; the penumbra area is where light is partially occluded. (b) Illustrate a shadow image example. (c) Illustrate the brightness curve at $H = 175$. The penumbra area is clear in this curve.

inputs. DeShadowNet (Qu et al. 2017) introduces an end-to-end shadow removal method containing a multi-branch fusion module. Additionally, several methods utilize Generative Adversarial Networks (GANs) (Goodfellow et al. 2014) for shadow removal tasks. ST-CGAN (Wang, Li, and Yang 2018) connects two GANs in sequence to jointly detect and remove shadows. DC-ShadowNet (Jin, Sharma, and Tan 2021) provides an unsupervised domain-classifier discriminator for guided shadow removal network. More recently, DeS3 (Jin et al. 2024) implemented a method capable of removing shadows that are cast on the object itself without requiring shadow mask inputs. However, due to the absence of additional shadow location information, their performance may degrade, and the number of parameters used could increase significantly. Different from these existing methods, we introduce a new concept “soft mask”, designed explicitly for shadow removal.

2.2 Shadow Detection

Shadow detection can be approached as a segmentation task, it often struggles with small shadows and indistinct shadow edges. Various methods have been proposed to address these challenges. BDRAR (Zhu et al. 2018) introduces a bidirectional pyramidal architecture for shadow detection. DSD (Zheng et al. 2019) designs a distraction-aware module to minimize false positives in shadow detection. Chen et al. (Chen et al. 2020) propose a task-specific semi-supervised learning mechanism to utilize unlabeled shadow images for detection, enhancing the robustness of the model. DHAN (Cun, Pun, and Shi 2020) is a well-used shadow detection model using dual hierarchical aggregation network training on synthetic shadow and shadow-free image pairs to improve detection accuracy. The SAM-Adapter (Chen et al. 2023) has been utilized to fine-tune the Segment Anything Model (SAM) (Kirillov et al. 2023) specifically for shadow detection tasks. While this approach improves accuracy, it demands a substantial number of model parameters. However, most existing methods detect shadows as binary masks and fail to represent the penumbra area. In contrast, our approach leverages the shadow removal loss and the Penumbra Formation Constraint loss, jointly training the shadow removal network and the shadow detection network.

3 Methods

In this section, we first explain the motivation behind our newly introduced soft shadow mask, inspired by the physical shadow formation model. We then propose the unified shadow removal framework *SoftShadow*, which leverages the powerful segmentation capabilities of SAM to produce both the soft shadow mask and shadow-free images. Finally, we introduce the penumbra formation constraint loss to assist the SAM and incorporate physical constraints.

3.1 Motivation

Shadow degradations in the real world exhibit considerable variation and can be classified into two main categories: soft shadows and hard shadows (Langer and Zucker 1997). This classification depends on the light source and the distance between the object and the surface, as shown in Figure 3(a). Soft shadows are characterized by blurred edges and gradual transitions from light to dark, creating penumbra areas, while hard shadows have sharp edges without penumbra.

Previous methods (Zhu et al. 2022; Fu et al. 2021; Guo et al. 2023a; Xiao et al. 2024) commonly use binary masks as guidance for shadow removal, effectively representing shadow locations with sharp edges. However, when applied to soft shadows with blurred boundaries, as shown in Figure 3 (b), binary masks struggle to fully capture these regions. The boundary between the shadow (umbra) and the non-shadow (lit) area is hard to determine. Additionally, we empirically observed that the decrease in brightness within the penumbra area (from lit to umbra area) is approximately linear, while the lit and umbra areas exhibit relatively uniform transitions, as shown in Figure 3(c).

Based on the observations, we use soft mask s instead of binary mask m . For a given shadow-free image x , shadow image y is formulated as:

$$y = a \cdot s \cdot x + (1 - s) \cdot x \quad (1)$$

where \cdot denotes element-wise multiplication, s is the soft shadow mask in which constant $s = 0$ represents lit area, $s = 1$ represents umbra area, and $s \in (0, 1)$ represents penumbra area. $a \in (0, 1)$ represents the illumination weight in the non-lit area. The newly formulated shadow degradation model offers the potential for modeling soft masks more effectively.

3.2 Overall Architecture of SoftShadow

SoftShadow is a unified framework designed to remove object shadows in images in an end-to-end manner. The overall architecture is illustrated in Figure 2. Within the SoftShadow framework, we leverage the segmentation capabilities of SAM by finetuning it to serve as our soft mask predictor. It was observed that the pretrained SAM often fails to produce object contours and accurately identify shadows (Jie and Zhang 2023). We use Low-Rank Adaptation (LoRA) (Hu et al. 2021) to finetune SAM with fewer trainable parameters and computational costs. We freeze all parameters in the image encoder and add a bypass on each self-attention block. Since the mask decoder is lightweight, we tune all the parameters of it.

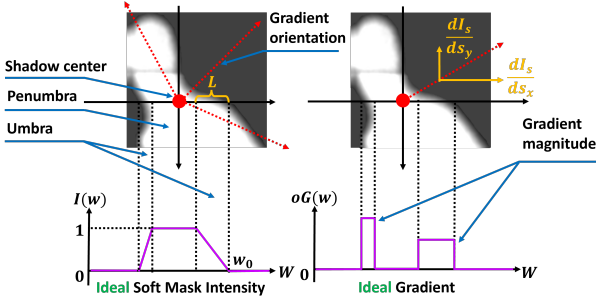


Figure 4: Illustrate the concept of Penumbra Formation Constraint. In the ideal soft shadow mask, the intensity in the penumbra area decreases progressively from the shadow center to the umbra area. The gradient orientation points from the shadow center towards the non-shadow area.

SAM is mainly trained for binary predictions, unlike the soft masks we aim to generate. To leverage SAM to generate continuous soft masks, we further introduce the penumbra formation constraints, i.e., using penumbra gradient loss \mathcal{L}_{pen} and mask reconstruction loss \mathcal{L}_{mask} to model the characteristics of soft masks in the penumbra area (details are described in Section 3.3). The constraints encourage the model to detect the shadow area and produce a continuous soft mask rather than a binary one, thereby capturing the shadow position more accurately.

Moreover, as shown in Figure 2, we feed the gradient of the shadow removal loss \mathcal{L}_{rem} back to SAM to jointly train SAM and the subsequent shadow removal network:

$$\mathcal{L}_{rem} = \mathbb{E}_n \|\hat{\mathbf{x}}_n - \mathbf{x}_n\|_F^2, \quad (2)$$

where n indexes all images, $\hat{\mathbf{x}}$ is the restored shadow-free image, and \mathbf{x} is the ground truth shadow-free image. To this end, the intermediate soft shadow masks can be refined using shadow removal results, with the SAM adaptor optimized for better location guidance in subsequent shadow removal. The overall training objective of the proposed SoftShadow framework is:

$$\mathcal{L} = \mathcal{L}_{mask} + \lambda_1 \mathcal{L}_{pen} + \lambda_2 \mathcal{L}_{rem}, \quad (3)$$

where λ_1 and λ_2 are the weighting coefficients to balance the influence of each term. With the merits of joint training and physical constraints, our SAM adaptor (LoRA) can effectively predict soft masks.

3.3 Penumbra Formation Constraint

We introduce the Penumbra Formation Constraint to enable SAM to predict the soft masks more accurately. According to the shadow formation (Nielsen and Madsen 2007) as shown in Figure 3 (a), the light intensity in the penumbra area depends on the distance between the object and the surface where the shadow is cast. For simplicity, the light intensity $I(w)$ at point w within the penumbra can be modeled by a linear function. As shown in Figure 4, we assume that the direction from the shadow center to the shadow outward is positive. The light intensity is $I(w) = I_0 \left(1 - \frac{w_0 - w}{L}\right)$,

where w is a pixel in the penumbra area, w_0 is the pixel at the edge between the penumbra and the lit area, and L is the width of the penumbra area in the certain direction. If set $I_0 = 1$, the soft mask intensity I_s can be written as:

$$I_s(w) = 1 - I(w) = \frac{w_0 - w}{L}. \quad (4)$$

The gradient of mask intensity is $\frac{dI_s}{dw} = -\frac{1}{L}$. The larger the absolute value of the gradient, the smaller the width L of the penumbra region, which represents a smaller predicted penumbra area. Based on Eq (4), we introduce a penumbra gradient constraint to help the model predict the penumbra area more clearly. This constraint aims to ensure that the gradient direction in the penumbra area radiates outward from the shadow center and the gradient magnitudes are finite (when hard mask, the gradient magnitude is infinite). Since modeling the gradient in all directions from the shadow center is impractical. We calculate the mask gradient in the horizontal and vertical directions. The loss function can be formulated as:

$$\mathcal{L}_{pen} = \mathbb{E}_{(n,p)} \left[R \left(o_x \frac{\partial I_{s_n}}{\partial x} \Big|_p \right) + R \left(o_y \frac{\partial I_{s_n}}{\partial y} \Big|_p \right) \right], \quad (5)$$

where n is the index of training images, and p is the pixel index in the penumbra area, R is the ReLU function (Nair and Hinton 2010). For a predicted soft mask, we assume it nearly represents a complete object and identifies the shadow center c . Based on this center, we determine the orientation vector o as:

$$o_x = \begin{cases} 1 & s_x < c_x, \\ -1 & s_x \geq c_x, \end{cases} \quad o_y = \begin{cases} 1 & s_y < c_y, \\ -1 & s_y \geq c_y, \end{cases} \quad (6)$$

In both Eq (5) and Eq (6), the variables o , s , and c represent coordinate points, where the subscripts x and y indicate the values along the horizontal and vertical axes, respectively. s represents the soft mask pixel in the penumbra area. We add a ReLU function to ignore pixels with values less than 0 and penalize the remaining values that are large, which indicates that the predicted intensity in the penumbra area changes quickly. We also employ a mask reconstruction loss \mathcal{L}_{mask} to enable SAM to identify the approximate soft shadow contour as follows:

$$\mathcal{L}_{mask} = \mathbb{E}_n \|\hat{\mathbf{s}} - \mathbf{s}_{gt}\|_F^2, \quad (7)$$

where n is the index of shadow masks, $\hat{\mathbf{s}}$ is the predicted soft shadow mask, and \mathbf{s}_{gt} is the ground truth soft shadow mask achieved by dividing the shadow-free image \mathbf{y} by the shadow image \mathbf{x} . Specifically, we convert \mathbf{y} and \mathbf{x} into YCbCr image space, using the Y channel to illustrate the brightness of these images, denoted as \mathbf{y}_Y and \mathbf{x}_Y , respectively. We then divide the \mathbf{y}_Y by \mathbf{x}_Y to obtain the difference between them, apply a low-pass filter f to reduce noise, and use a threshold to eliminate outliers as follows:

$$\mathbf{s}_{gt} = \max \left(t, f \left(\frac{\mathbf{x}_Y}{\mathbf{y}_Y} \right) \right), \quad (8)$$

	Methods	Input Masks	shadow			non-shadow			all		
			PSNR \uparrow	SSIM \uparrow	MAE \downarrow	PSNR \uparrow	SSIM \uparrow	MAE \downarrow	PSNR \uparrow	SSIM \uparrow	MAE \downarrow
SRD	DHAN	DHAN	33.67	0.978	8.94	34.79	0.979	4.80	30.51	0.949	5.67
	DC-ShadowNet	NA	34.00	0.975	7.70	35.53	0.981	3.65	31.53	0.955	4.65
	BMNet	DHAN	35.05	0.981	6.61	36.02	0.982	3.61	31.69	0.956	4.46
	ShadowFormer	DHAN	35.55	0.982	6.14	36.82	0.983	3.54	32.46	0.957	4.28
	ShadowDiffusion	DHAN	38.72	0.987	4.98	37.78	0.985	3.44	34.73	0.970	3.63
	Inpaint4Shadow	DHAN	36.73	0.985	5.70	36.70	0.985	3.27	33.27	0.967	3.81
	DeS3	NA	37.91	0.986	5.27	37.45	0.984	3.03	34.11	0.968	3.56
	Homoformer	DHAN	<u>38.81</u>	<u>0.987</u>	4.25	39.45	<u>0.988</u>	<u>2.85</u>	<u>35.37</u>	<u>0.972</u>	<u>3.33</u>
	SAM-helps-shadow	NA	33.94	0.979	7.44	33.85	0.981	3.74	30.72	0.952	4.79
	ours	NA	39.08	0.989	<u>4.33</u>	<u>39.36</u>	0.992	2.58	35.57	0.975	3.11
ISTD+	BMNet	GT	37.87	0.991	5.62	37.51	0.985	2.45	33.98	0.972	2.97
	ShadowDiffusion	GT	39.69	0.992	4.97	38.89	0.987	2.28	35.67	0.975	2.72
	HomoFormer	GT	39.49	0.993	4.73	38.75	0.984	2.23	35.35	0.975	2.64
	DC-ShadowNet	NA	31.06	0.976	12.62	27.03	0.961	6.82	25.03	0.926	7.77
	DeS3	NA	36.49	0.989	6.56	34.70	0.972	3.40	31.38	0.958	3.94
	BMNet	FDRNet	-	-	6.1	-	-	2.9	-	-	3.5
	ShadowDiffusion	FDRNet	<u>40.12</u>	<u>0.992</u>	<u>5.15</u>	<u>36.66</u>	<u>0.978</u>	<u>2.74</u>	<u>34.08</u>	<u>0.968</u>	<u>3.12</u>
	HomoFormer	FDRNet	38.84	0.991	5.31	34.58	0.966	3.17	32.41	0.953	3.51
	Ours	NA	40.36	0.993	4.78	37.89	0.982	2.46	35.00	0.972	2.85

Table 1: The quantitative results of shadow removal using our SoftShadow and recent methods on SRD and ISTD+ datasets. The ‘‘Input Masks’’ column shows the different types of input masks used by these methods. ‘‘NA’’ means the method does not require masks as input. ‘‘GT’’ means the method uses manually annotated ground truth mask as input. The best and the second results are **boldfaced** and underlined, respectively.

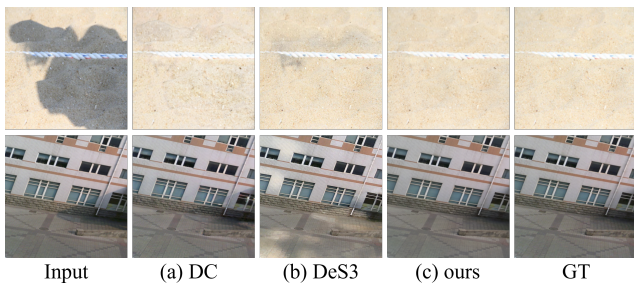


Figure 5: Examples of shadow removal results on SRD datasets (Qu et al. 2017). The input shadow image, the estimated results of (a) DC-ShadowNet (Jin, Sharma, and Tan 2021), (b) DeS3 (Jin et al. 2024), and (c) Ours, as well as the ground truth image, respectively.

where t is the threshold used to define the outer boundary between the penumbra area and the lit area.

4 Experiments

4.1 Experimental Setups

Implementation details The shadow removal backbone in our SoftShadow framework can be any shadow removal network. We use ShadowDiffusion (Guo et al. 2023b) as the backbone example for all experiments. We empirically set the threshold $t = 0.76$ to get the ground truth soft shadow mask s_{gt} . We employ the ViT-H model as the backbone for SAM (Kirillov et al. 2023). A set of LoRA (Hu et al. 2021) layers with a rank of 8 is added to the self-attention blocks

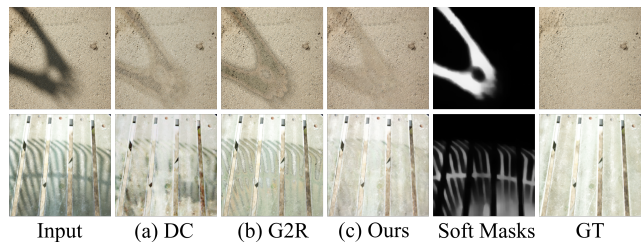


Figure 6: Examples of shadow removal results on the LRSS dataset (Gryka, Terry, and Brostow 2015). The input shadow image, the estimated results of (a) DC-ShadowNet (Jin, Sharma, and Tan 2021), (b) G2R-ShadowNet (Liu et al. 2021), (c) Ours, our predicted soft shadow masks and ground truth image, respectively.

in the image encoder of SAM. We set $\lambda_1 = 0.1$ and $\lambda_2 = 1$. For evaluation, we use the DDIM sampler (Song, Meng, and Ermon 2020) and 5 diffusion sampling steps. The training batch size is 16. For more training details, please refer to the **supplementary**.

Benchmark datasets We work with four benchmark datasets for the various shadow removal experiments. **SRD Dataset** (Qu et al. 2017) consists of 2,680 training pairs and 408 testing pairs of shadow and shadow-free images. Notably, the SRD dataset does not provide shadow masks, the previous methods using SRD commonly using masks detected by DHAN (Cun, Pun, and Shi 2020) methods. **LRSS Dataset** (Gryka, Terry, and Brostow 2015) is a specifically

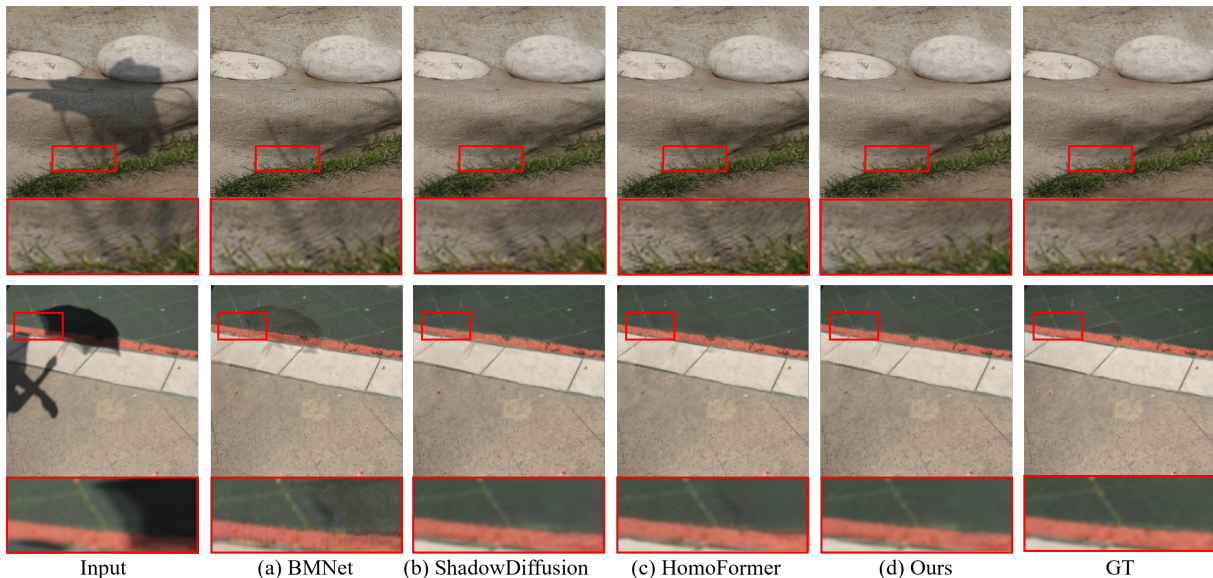


Figure 7: Examples of soft shadow image removal results on the SRD dataset (Qu et al. 2017). The input shadow image, the estimated results of (a) BMNet (Zhu et al. 2022), (b) ShadowDiffusion (Guo et al. 2023b), (c) Homoformer (Xiao et al. 2024), and (d) Ours, as well as the ground truth image, respectively.

designed soft shadow dataset that includes 137 images. We select 48 paired shadow and shadow-free images as our testing set. **UIUC Dataset** (Guo, Dai, and Hoiem 2012) contains 76 pairs of images for testing. It features a variety of shadow types (Jin et al. 2024), including soft, hard, and self shadows, which provides a diverse and challenging set of conditions for evaluating shadow removal methods. **ISTD+ Dataset** (Le and Samaras 2019) is adjusted ISTD dataset (Wang, Li, and Yang 2018), reducing the illumination inconsistency between shadow and shadow-free images of the ISTD dataset. It manually annotated binary masks.

Evaluation metrics Following previous works (Cun, Pun, and Shi 2020; Guo et al. 2023b; Xiao et al. 2024), we employ the Peak Signal-to-Noise Ratio (PSNR), Structural Similarity Index (SSIM) (Wang et al. 2004), and Mean Absolute Error (MAE) (Willmott and Matsuura 2005) as quantitative evaluation metrics. We also calculate all metrics for shadow areas, non-shadow areas, and all pixels between ground truth shadow-free images and generated removal results.

4.2 Comparison with State-of-the-Art

We compare our proposed method with several state-of-the-art shadow removal methods. We include methods that do not require shadow masks as input, e.g., DC-shadowNet (Jin, Sharma, and Tan 2021), DeS3 (Jin et al. 2024), and SAM-helps-shadow (Zhang, Gu, and Zhu 2023). And methods that require shadow masks, including DHAN (Cun, Pun, and Shi 2020), BMNet (Zhu et al. 2022), ShadowFormer (Guo et al. 2023a), Inpaint4Shadow (Li et al. 2023), ShadowDiffusion (Guo et al. 2023b) and Homoformer (Xiao et al. 2024). To demonstrate the generalizability of our method, we also compare it with zero-shot methods including BCDiff (Guo et al. 2023c) and G2R-ShadowNet (Liu et al. 2021) on the LRSS (Gryka, Terry, and Brostow 2015) and UIUC (Guo,

Dai, and Hoiem 2012) datasets.

Quantitative results Table 1 shows the quantitative results of SRD and ISTD+ datasets. The SRD dataset contains many soft shadow images, which is more suitable for validating our methods. Specifically, we outperform all competing methods over all metrics, whether they require input shadow masks or not. Compared with the most recent work without requiring mask input, i.e., DeS3 (Jin et al. 2024), the PSNR is improved from 34.11 dB to 35.57 dB in whole images. When comparing with methods that need input masks, we outperform the SOTA method Homoformer (Xiao et al. 2024), which uses DHAN (Cun, Pun, and Shi 2020) mask as their input. On the ISTD+ dataset, we significantly outperform DeS3 (Jin et al. 2024), increasing the PSNR from 31.38 dB to 35.00 dB. For methods that rely on the ground truth masks from the ISTD+ dataset, we evaluate them using masks detected by the FDRNet (Zhu et al. 2021) followed by previous methods BMNet (Zhu et al. 2022), to ensure a fair comparison. We outperform all competing methods under the condition of without ground truth manually annotated masks. Besides, we even achieve comparable results against some SOTA methods using ground truth masks as shown in Table 1. To further evaluate the boundary artifacts suppress ability on SRD dataset, we present the restoration results in the penumbra area in Table 3. The penumbra area is obtained using the method from AEF (Fu et al. 2021). For methods that require binary masks as input, such as Homoformer, our penumbra area provides much better results.

Table 2 shows the generalizability of our methods. We use our pretrained model on the SRD dataset and test it on LRSS and UIUC datasets without further training. The DeS3 (Jin et al. 2024) has better results because they train their method on the LRSS training set. For comparison, we chose DC-ShadowNet as our baseline since this method does

Methods	LRSS			UIUC		
	PSNR \uparrow	SSIM \uparrow	MAE \downarrow	PSNR \uparrow	SSIM \uparrow	MAE \downarrow
DC	20.89	0.902	12.55	24.85	0.849	9.51
G2R	20.90	0.901	9.99	27.56	0.858	7.43
BCDiff	22.13	0.922	10.68	26.81	0.852	7.96
Ours	23.32	0.933	9.77	28.85	0.903	6.48

Table 2: The quantitative results of shadow removal using our SoftShadow and recent methods on the LRSS dataset. Here, ‘‘DC’’ refer to DC-ShadowNet (Jin, Sharma, and Tan 2021), ‘‘G2R’’ refer to G2R-ShadowNet. The best results are **boldfaced**.

Methods	PSNR	MAE
Inpaint4Shadow	40.10	4.23
DeS3	40.91	4.08
HomoFormer	40.82	3.91
Ours	41.84	3.77

Table 3: The quantitative results in the penumbra area. The best results are **boldfaced**.

not require masks as input. Our results significantly outperform DC-ShadowNet on LRSS and UIUC datasets. Additionally, we compare our methods with two zero-shot methods, which are designed to have better generalizability. The results demonstrate that our method has the best PSNR/SSIM/MAE among the comparison methods.

Qualitative evaluation To further demonstrate the effectiveness of our methods compared to other competing methods, Figure 7 illustrates our improvements in removing soft shadows on the SRD dataset compared with methods using binary shadow masks. The soft masks typically appear as soft boundaries of large object shadows or in small shadow regions. Specifically, our samples demonstrate that we effectively remove both types of soft shadows while preserving the illumination transition in penumbra areas. Figure 5 shows our improvement in shadow area accuracy compared to other end-to-end methods. Our approach effectively removes all parts of the shadow shown in the first row. In the second row, we successfully remove shadows in regions with complex textures. Figure 6 highlights our method’s generalizability on the LRSS dataset. The results demonstrate that our method achieves better shadow removal performance without further training on the LRSS dataset.

5 Ablation Study

We ablate our method, SoftShadow, by removing two losses: the mask reconstruction loss \mathcal{L}_{mask} and the penumbra gradient loss \mathcal{L}_{pen} , and demonstrate the results on SRD and LRSS datasets. First, we finetune the framework using only the shadow removal loss \mathcal{L}_{rem} . The results show that without shadow mask guidance, SAM struggles to detect shadow masks in some cases. Next, we add the mask reconstruction loss \mathcal{L}_{mask} to provide SAM with more precise mask position guidance. The results indicate that the \mathcal{L}_{mask} improves shadow removal performance. Finally, we added the penumbra gradient loss \mathcal{L}_{pen} to refine the mask boundary. Accord-

Methods	LRSS			SRD		
	PSNR \uparrow	SSIM \uparrow	MAE \downarrow	PSNR \uparrow	SSIM \uparrow	MAE \downarrow
SAM	21.78	0.913	12.07	35.27	0.973	3.32
\mathcal{L}_{mask}	23.08	0.935	9.97	35.44	0.974	3.17
Ours	23.32	0.933	9.77	35.57	0.975	3.11

Table 4: The ablation studies for the mask reconstruction loss \mathcal{L}_{mask} and the constraint loss \mathcal{L}_{pen} in LRSS and SRD datasets. Here, the ‘‘SAM’’ means pretrained SAM. The best results are **boldfaced**.

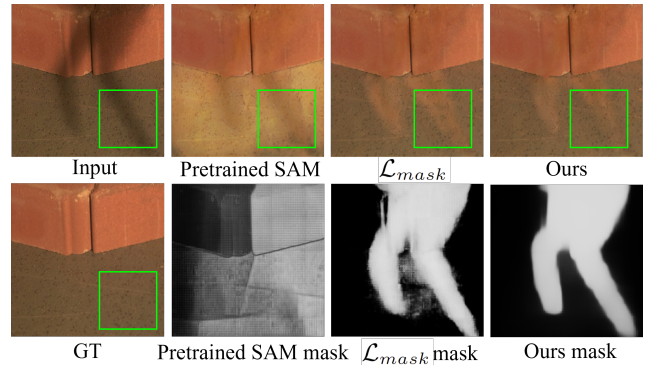


Figure 8: The quantitative results of shadow removal and their predicted masks with Pretrained SAM, \mathcal{L}_{mask} , and $\mathcal{L}_{mask} + \mathcal{L}_{pen}$ (Ours), respectively.

ing to Table 4, we can see that in the LRSS dataset, both \mathcal{L}_{mask} and \mathcal{L}_{pen} significantly improve performance, but in the SRD dataset, \mathcal{L}_{pen} does not show much improvement in terms of PSNR. We hypothesize that it might be caused by the proportion of soft areas in the SRD dataset is relatively small, so metrics like PSNR, which measure the average error, may not reflect the improvements. As shown in Figure 8, adding the constraint loss \mathcal{L}_{pen} results in more accurate and smoother soft mask contour compared to using only \mathcal{L}_{mask} , leading to better results in soft shadow areas. From the perspective of the removal network, the constraint loss provides more detailed soft boundary information, leading to better results in soft shadow areas.

6 Conclusion

In this paper, we introduce novel soft shadow masks designed specifically for shadow removal. To achieve this, we propose a unified framework, *SoftShadow*, that eliminates the need for additional shadow mask input. By leveraging a pre-trained SAM with LoRA, the framework accurately predicts soft masks as intermediate results, capturing detailed and varied shadow information. Additionally, we introduce a penumbra formation constraint, inspired by the physical shadow formation model, to jointly tune SAM and the shadow removal network, refining the soft mask in the penumbra area and facilitating artifact-free restoration. Extensive experiments demonstrate that our method is superior on various occasions, proving the validity of our method.

References

- Chen, T.; Zhu, L.; Deng, C.; Cao, R.; Wang, Y.; Zhang, S.; Li, Z.; Sun, L.; Zang, Y.; and Mao, P. 2023. Sam-adapter: Adapting segment anything in underperformed scenes. In *Proceedings of the IEEE/CVF International Conference on Computer Vision*, 3367–3375.
- Chen, Z.; Zhu, L.; Wan, L.; Wang, S.; Feng, W.; and Heng, P.-A. 2020. A multi-task mean teacher for semi-supervised shadow detection. In *Proceedings of the IEEE/CVF Conference on computer vision and pattern recognition*, 5611–5620.
- Cun, X.; Pun, C.-M.; and Shi, C. 2020. Towards ghost-free shadow removal via dual hierarchical aggregation network and shadow matting gan. In *Proceedings of the AAAI Conference on Artificial Intelligence*, volume 34, 10680–10687.
- Dosovitskiy, A.; Beyer, L.; Kolesnikov, A.; Weissenborn, D.; Zhai, X.; Unterthiner, T.; Dehghani, M.; Minderer, M.; Heigold, G.; Gelly, S.; et al. 2020. An image is worth 16x16 words: Transformers for image recognition at scale. *arXiv preprint arXiv:2010.11929*.
- Fu, L.; Zhou, C.; Guo, Q.; Juefei-Xu, F.; Yu, H.; Feng, W.; Liu, Y.; and Wang, S. 2021. Auto-exposure fusion for single-image shadow removal. In *Proceedings of the IEEE/CVF conference on computer vision and pattern recognition*, 10571–10580.
- Goodfellow, I.; Pouget-Abadie, J.; Mirza, M.; Xu, B.; Warde-Farley, D.; Ozair, S.; Courville, A.; and Bengio, Y. 2014. Generative adversarial nets. *Advances in neural information processing systems*, 27.
- Gryka, M.; Terry, M.; and Brostow, G. J. 2015. Learning to remove soft shadows. *ACM Transactions on Graphics (TOG)*, 34(5): 1–15.
- Guo, L.; Huang, S.; Liu, D.; Cheng, H.; and Wen, B. 2023a. ShadowFormer: Global context helps shadow removal. In *Proceedings of the AAAI Conference on Artificial Intelligence*, volume 37, 710–718.
- Guo, L.; Wang, C.; Wang, Y.; Huang, S.; Yang, W.; Kot, A. C.; and Wen, B. 2024. Single-Image Shadow Removal Using Deep Learning: A Comprehensive Survey. *arXiv preprint arXiv:2407.08865*.
- Guo, L.; Wang, C.; Yang, W.; Huang, S.; Wang, Y.; Pfister, H.; and Wen, B. 2023b. Shadowdiffusion: When degradation prior meets diffusion model for shadow removal. In *Proceedings of the IEEE/CVF Conference on Computer Vision and Pattern Recognition*, 14049–14058.
- Guo, L.; Wang, C.; Yang, W.; Wang, Y.; and Wen, B. 2023c. Boundary-aware divide and conquer: A diffusion-based solution for unsupervised shadow removal. In *Proceedings of the IEEE/CVF International Conference on Computer Vision*, 13045–13054.
- Guo, R.; Dai, Q.; and Hoiem, D. 2012. Paired regions for shadow detection and removal. *IEEE transactions on pattern analysis and machine intelligence*, 35(12): 2956–2967.
- Ho, J.; Jain, A.; and Abbeel, P. 2020. Denoising diffusion probabilistic models. *Advances in neural information processing systems*, 33: 6840–6851.
- Hu, E. J.; Shen, Y.; Wallis, P.; Allen-Zhu, Z.; Li, Y.; Wang, S.; Wang, L.; and Chen, W. 2021. Lora: Low-rank adaptation of large language models. *arXiv preprint arXiv:2106.09685*.
- Jie, L.; and Zhang, H. 2023. When SAM meets shadow detection. *arXiv preprint arXiv:2305.11513*.
- Jin, Y.; Sharma, A.; and Tan, R. T. 2021. Dc-shadownet: Single-image hard and soft shadow removal using unsupervised domain-classifier guided network. In *Proceedings of the IEEE/CVF International Conference on Computer Vision*, 5027–5036.
- Jin, Y.; Ye, W.; Yang, W.; Yuan, Y.; and Tan, R. T. 2024. DeS3: Adaptive Attention-Driven Self and Soft Shadow Removal Using ViT Similarity. In *Proceedings of the AAAI Conference on Artificial Intelligence*, volume 38, 2634–2642.
- Kirillov, A.; Mintun, E.; Ravi, N.; Mao, H.; Rolland, C.; Gustafson, L.; Xiao, T.; Whitehead, S.; Berg, A. C.; Lo, W.-Y.; et al. 2023. Segment anything. In *Proceedings of the IEEE/CVF International Conference on Computer Vision*, 4015–4026.
- Langer, M. S.; and Zucker, S. W. 1997. What is a light source? In *Proceedings of IEEE Computer Society Conference on Computer Vision and Pattern Recognition*, 172–178. IEEE.
- Le, H.; and Samaras, D. 2019. Shadow removal via shadow image decomposition. In *Proceedings of the IEEE/CVF International Conference on Computer Vision*, 8578–8587.
- Li, X.; Guo, Q.; Abdelfattah, R.; Lin, D.; Feng, W.; Tsang, I.; and Wang, S. 2023. Leveraging inpainting for single-image shadow removal. In *Proceedings of the IEEE/CVF International Conference on Computer Vision*, 13055–13064.
- Liu, Y.; Ke, Z.; Xu, K.; Liu, F.; Wang, Z.; and Lau, R. W. 2024. Recasting regional lighting for shadow removal. In *Proceedings of the AAAI Conference on Artificial Intelligence*, volume 38, 3810–3818.
- Liu, Z.; Yin, H.; Wu, X.; Wu, Z.; Mi, Y.; and Wang, S. 2021. From shadow generation to shadow removal. In *Proceedings of the IEEE/CVF conference on computer vision and pattern recognition*, 4927–4936.
- Nair, V.; and Hinton, G. E. 2010. Rectified linear units improve restricted boltzmann machines. In *Proceedings of the 27th international conference on machine learning (ICML-10)*, 807–814.
- Nielsen, M.; and Madsen, C. B. 2007. Segmentation of soft shadows based on a daylight-and-penumbral model. In *International Conference on Computer Vision/Computer Graphics Collaboration Techniques and Applications*, 341–352. Springer.
- Qu, L.; Tian, J.; He, S.; Tang, Y.; and Lau, R. W. 2017. Dshadownet: A multi-context embedding deep network for shadow removal. In *Proceedings of the IEEE conference on computer vision and pattern recognition*, 4067–4075.
- Saharia, C.; Ho, J.; Chan, W.; Salimans, T.; Fleet, D. J.; and Norouzi, M. 2022. Image super-resolution via iterative refinement. *IEEE transactions on pattern analysis and machine intelligence*, 45(4): 4713–4726.

Song, J.; Meng, C.; and Ermon, S. 2020. Denoising diffusion implicit models. *arXiv preprint arXiv:2010.02502*.

Vaswani, A.; Shazeer, N.; Parmar, N.; Uszkoreit, J.; Jones, L.; Gomez, A. N.; Kaiser, Ł.; and Polosukhin, I. 2017. Attention is all you need. *Advances in neural information processing systems*, 30.

Wang, J.; Li, X.; and Yang, J. 2018. Stacked conditional generative adversarial networks for jointly learning shadow detection and shadow removal. In *Proceedings of the IEEE conference on computer vision and pattern recognition*, 1788–1797.

Wang, Z.; Bovik, A. C.; Sheikh, H. R.; and Simoncelli, E. P. 2004. Image quality assessment: from error visibility to structural similarity. *IEEE transactions on image processing*, 13(4): 600–612.

Willmott, C. J.; and Matsuura, K. 2005. Advantages of the mean absolute error (MAE) over the root mean square error (RMSE) in assessing average model performance. *Climate research*, 30(1): 79–82.

Xiao, J.; Fu, X.; Zhu, Y.; Li, D.; Huang, J.; Zhu, K.; and Zha, Z.-J. 2024. HomoFormer: Homogenized Transformer for Image Shadow Removal. In *Proceedings of the IEEE/CVF Conference on Computer Vision and Pattern Recognition*, 25617–25626.

Zhang, X.; Gu, C.; and Zhu, S. 2023. Sam-helps-shadow: When segment anything model meet shadow removal. *arXiv e-prints*, arXiv–2306.

Zheng, Q.; Qiao, X.; Cao, Y.; and Lau, R. W. 2019. Distraction-aware shadow detection. In *Proceedings of the IEEE/CVF conference on computer vision and pattern recognition*, 5167–5176.

Zhu, L.; Deng, Z.; Hu, X.; Fu, C.-W.; Xu, X.; Qin, J.; and Heng, P.-A. 2018. Bidirectional feature pyramid network with recurrent attention residual modules for shadow detection. In *Proceedings of the European Conference on Computer Vision (ECCV)*, 121–136.

Zhu, L.; Xu, K.; Ke, Z.; and Lau, R. W. 2021. Mitigating intensity bias in shadow detection via feature decomposition and reweighting. In *Proceedings of the IEEE/CVF International Conference on Computer Vision*, 4702–4711.

Zhu, Y.; Huang, J.; Fu, X.; Zhao, F.; Sun, Q.; and Zha, Z.-J. 2022. Bijective mapping network for shadow removal. In *Proceedings of the IEEE/CVF Conference on Computer Vision and Pattern Recognition*, 5627–5636.